Supporting Information

Table of contents

S1. General

Instruments

^{1}H- and ^{13}C-nuclear magnetic resonance (NMR) spectroscopies were obtained on a Bruker Avance III HD NanoBay 400 FT-NMR spectrometers using tetramethylsilane (^{1}H-NMR) and solvent residual peaks (^{13}C-NMR) as internal standards. Melting points (Mp) were determined on a Yanaco micro melting point apparatus MP-500D. Elemental analyses (EA) were performed on an Elementar vario EL cube in the CHN mode. Ultraviolet-visible (UV-vis) absorption spectra were recorded on a Shimadzu UV-1650 spectrophotometer in $CHCl_3$ (10^{-5} M). Cyclic voltammetry (CV) measurements were carried out on a BAS 2323 bipotentiostat using a platinum disk working electrode, a platinum wire counter electrode, and a Ag/Ag$^+$ reference electrode in a standard three-electrode cell. The voltammograms were collected in 0.1 M *o*-DCB /PhCN mixed solution of tetrabutylammonium hexafluorophosphate (Bu_4NPF_6), and the voltage-current characteristic was obtained at the scan rate of 100 mV/s. Redox potentials were calibrated using the ferrocene/ferrocenium (Fc/Fc$^+$) redox couple to be 4.8 eV below the vacuum. Theoretical calculations were performed on Gaussian 09W (Revision C.01) package of programs.[1] The ground state structure was optimized with DFT calculation at the B3LYP/6-31G(d,p) level of theory. The theoretical absorption bands were estimated by TD-DFT calculation at the B3LYP/6-31G(d,p) level of theory. OFET measurements were performed in a vacuum or under ambient conditions. Electron mobilities (μ_e) were determined from the equation $I_{DS} = W/(2L)C_i\mu_e(V_{GS}-V_{th})$,[2] where I_{DS}, W, L, C_i, V_{GS}, and V_{th} are the source–drain current, channel width (38 mm), channel length (5 μm), capacitance of the SiO_2 dielectric layers (10 nF·cm^{-2}), gate voltage, and threshold gate voltage, respectively. Grazing-incidence X-ray diffraction (GI-XRD) measurements were taken by an X-ray diffractometer FR-E equipped with a two-dimensional detector R-axis IV (Rigaku) involving an imaging plate (Fujifilm). Beam of 0.3-mm collimated Cu Ka radiation (l = 1.5418 Å) was used as an X-ray, and the camera length was set at 250 mm. Film samples were placed onto a pulse motor stage and covered with a handmade chamber to control a relative humidity around the samples. An incident angle of the beam to the substrate surface was adjusted at ca. 0.18−0.22° by using a Z pulse motor stage ALV-300-HM and an oblique pulse motor stage ATS-C310-EM (Chuo Precision Industrial). X-ray exposed times were set at 30 min for each film prepared onto a HMDS-treated substrate. Atomic force microscopy (AFM) imaging was performed in a tapping mode under ambient conditions with an Oxford Instruments MFP-3D.

S2. NICS(0) values and conformation of target compounds

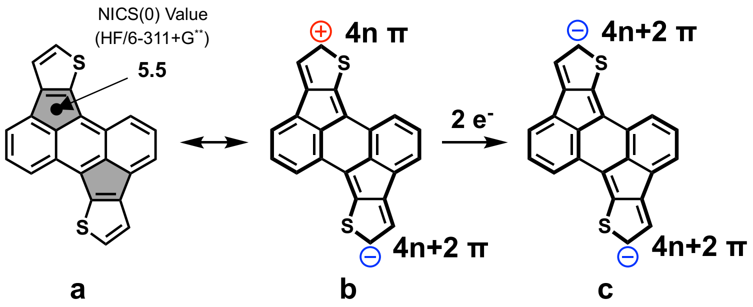

Figure S1. NICS(0) value of dithiarubicene and representation of aromaticity.

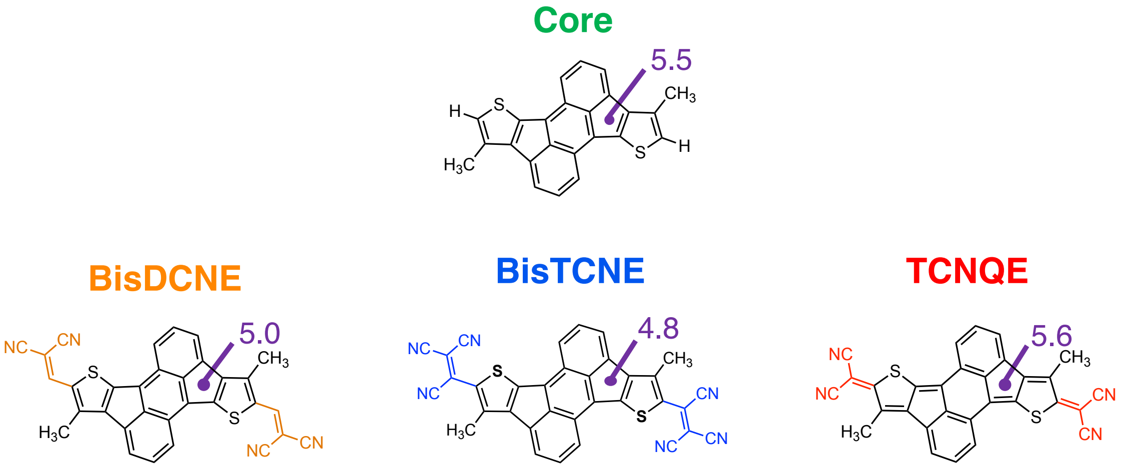

Figure S2. NICS(0) values (purple number) for four compounds calculated at the HF/6-311+G**//B3LYP/6-31G** level of theory.

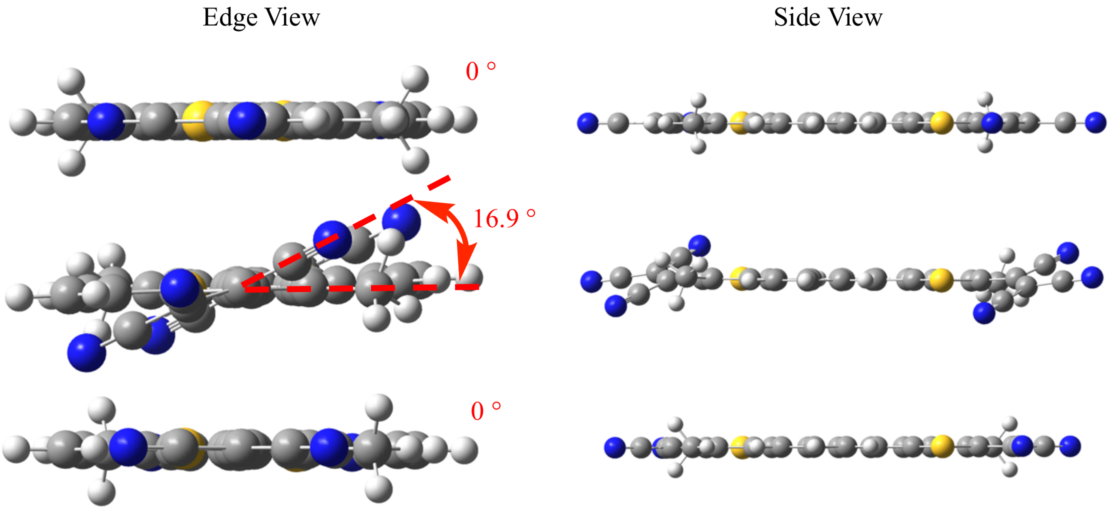

Figure S3. Dihedral angles between **Core** and substituents estimated by using DFT calculation (B3LYP/6-31G**). **BisDCNE**: top, **BisTCNE**: middle, and **TCNQE**: bottom.

S3. TD-DFT calculations

Table S1. Comparison of absorption bands between the observed value and theoretical value estimated by TD-DFT calculation (B3LYP/6-31G**).[1]

Compound	λ_{obsd} [nm]	λ_{cacld} [nm]	Oscillator strength
Core	615	648	0.12
BisDCNE	646	689	0.54
BisTCNE	653	683	0.73
TCNQE	738	712	0.79

S4. OFET characteristics

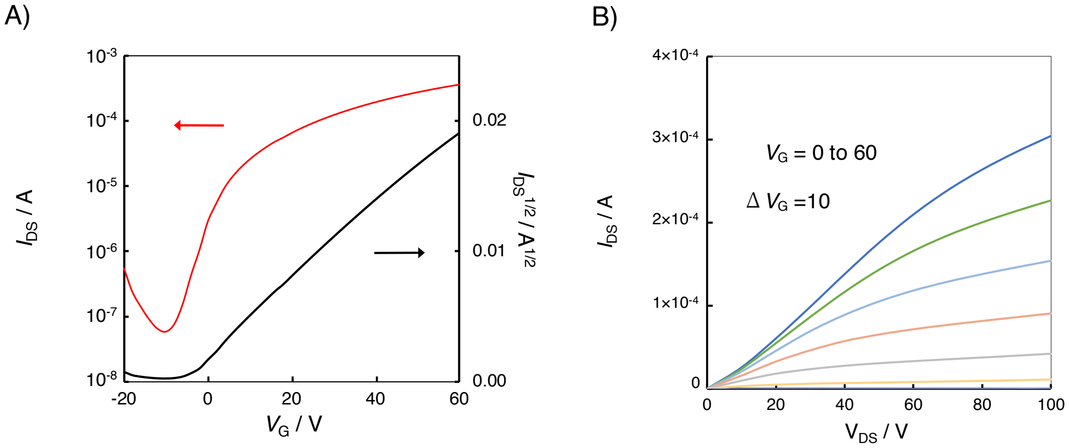

Figure S4. (A) Transfer and (B) output plots of **BisDCNE**-based OFET device fabricated on HMDS-treated SiO_2 insulation surface after the thermal annealing at 100 °C.

S5. 2D GIXRD images

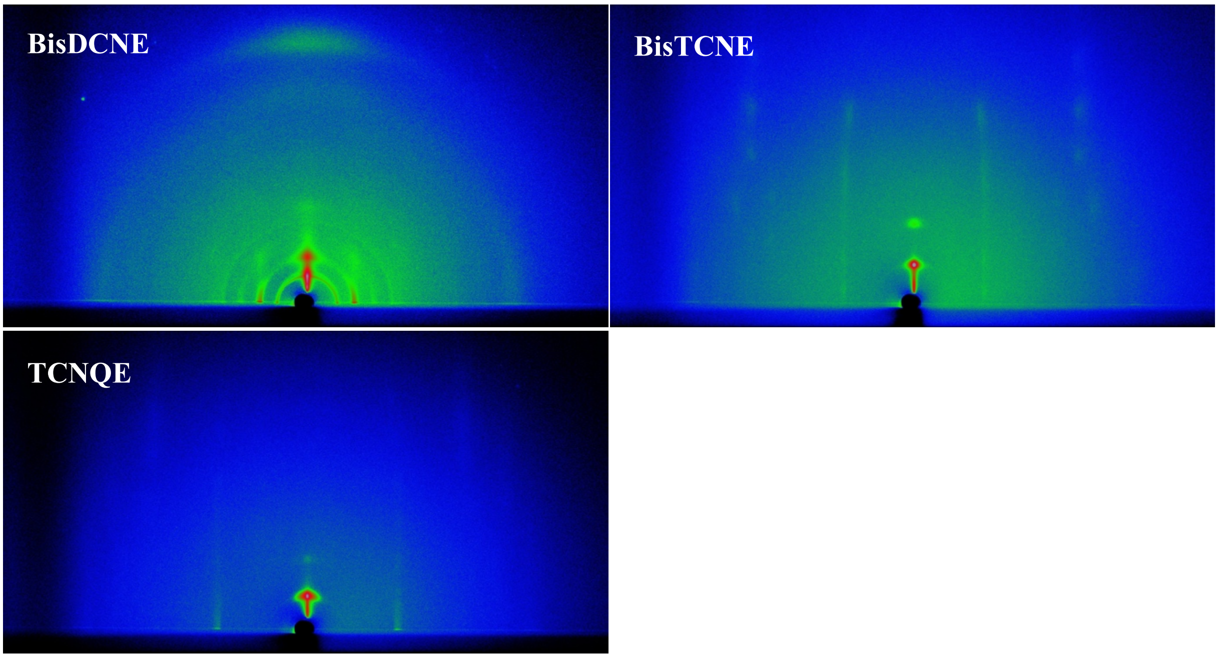

Figure S5. 2D GIXRD images of thin films fabricated on HMDS-treated SiO_2 insulation surface after the thermal annealing.

S6. AFM images

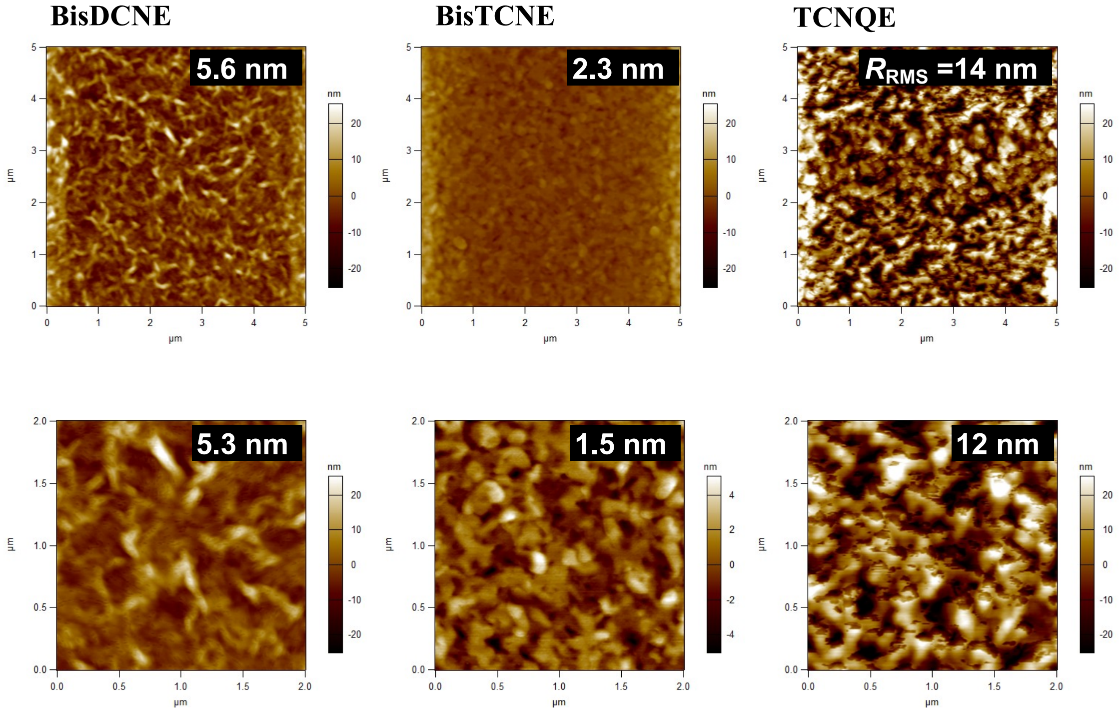

Figure S6. AFM images of the device surfaces between the electrodes after the thermal annealing. The inset values indicate the root mean square roughness (R_{RMS}) calculated each image.

S7. NMR spectra

Core

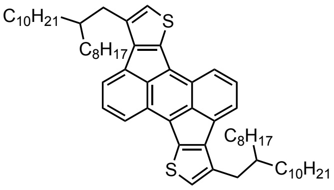

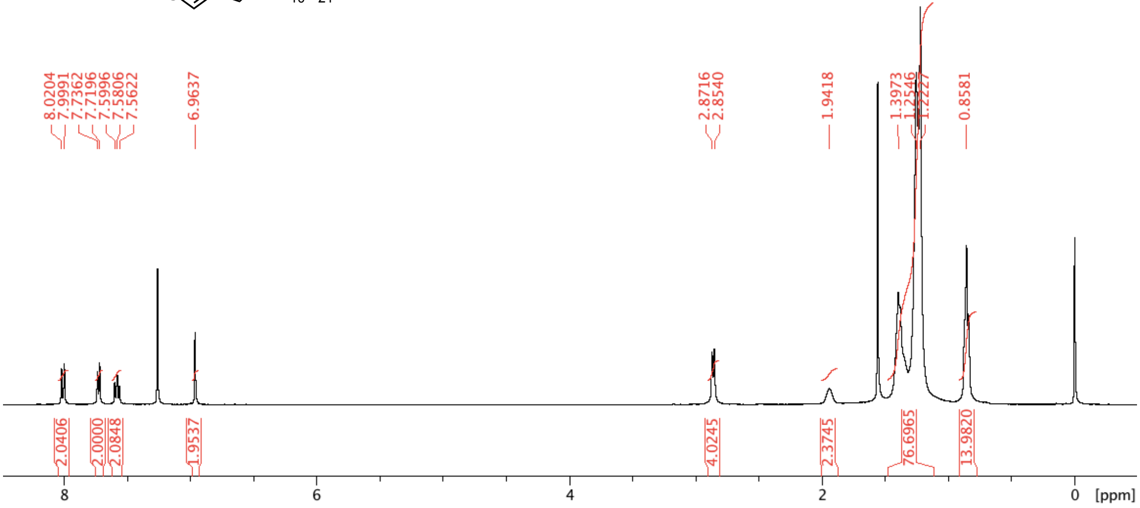

Diformyl-Core (1)

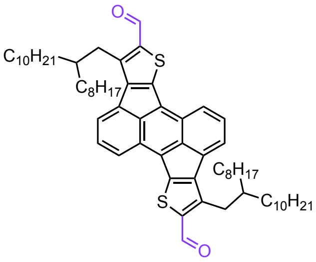

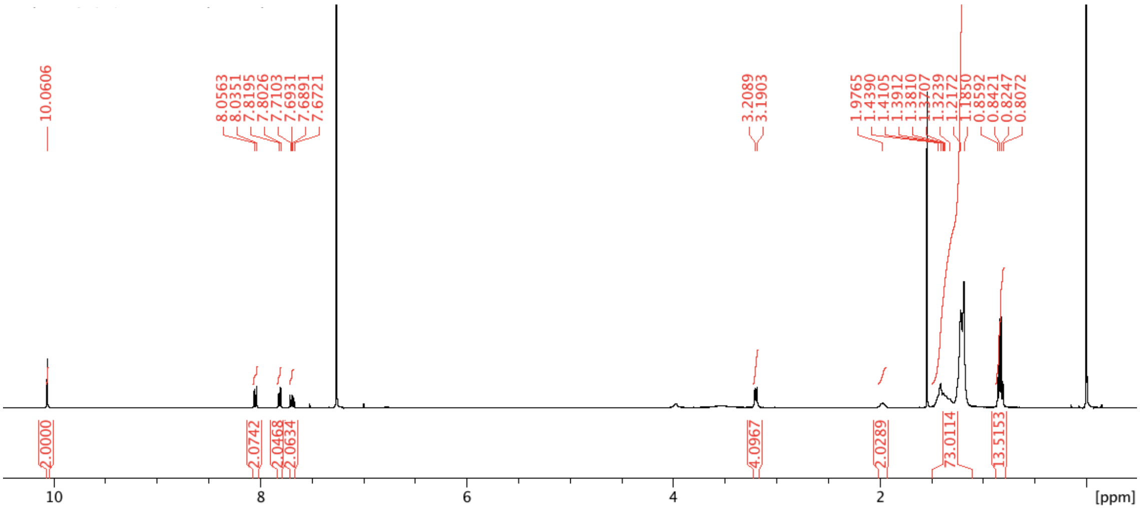

BisDCNE

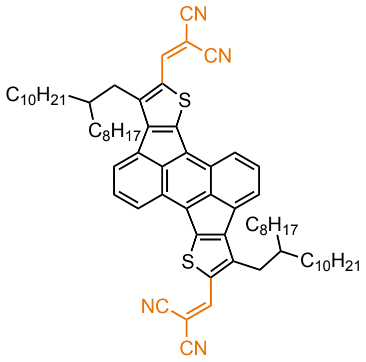
CN
CN
$C_{10}H_{21}$
S
C_8H_{17}
C_8H_{17}
S
$C_{10}H_{21}$
NC
CN

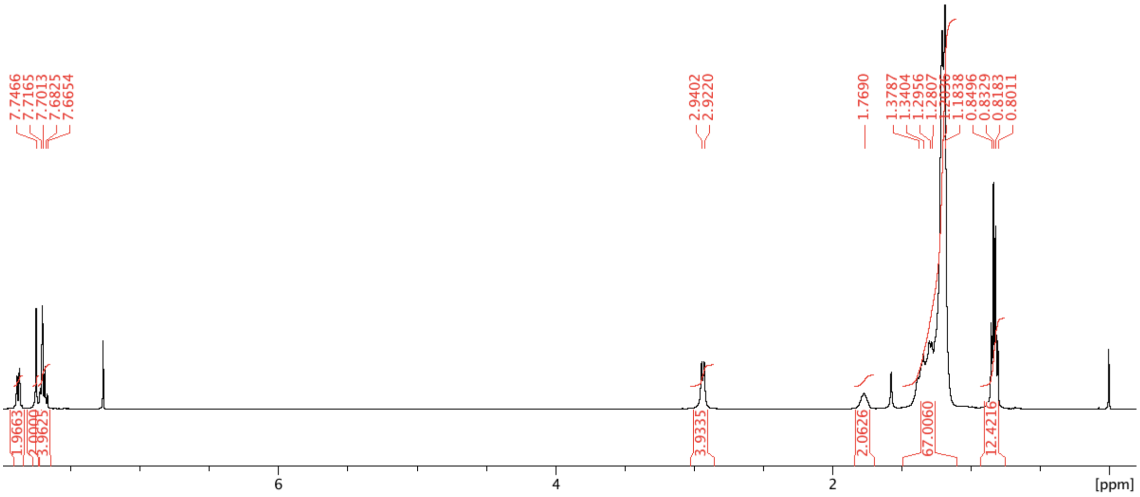
7.7466
7.7165
7.7013
7.6825
7.6654
2.9402
2.9220
1.7690
1.3787
1.3404
1.2956
1.2807
1.2036
1.1838
0.8496
0.8329
0.8183
0.8011
1.9663
2.0000
3.9625
3.9335
2.0626
67.0060
12.4216
6
4
2
[ppm]

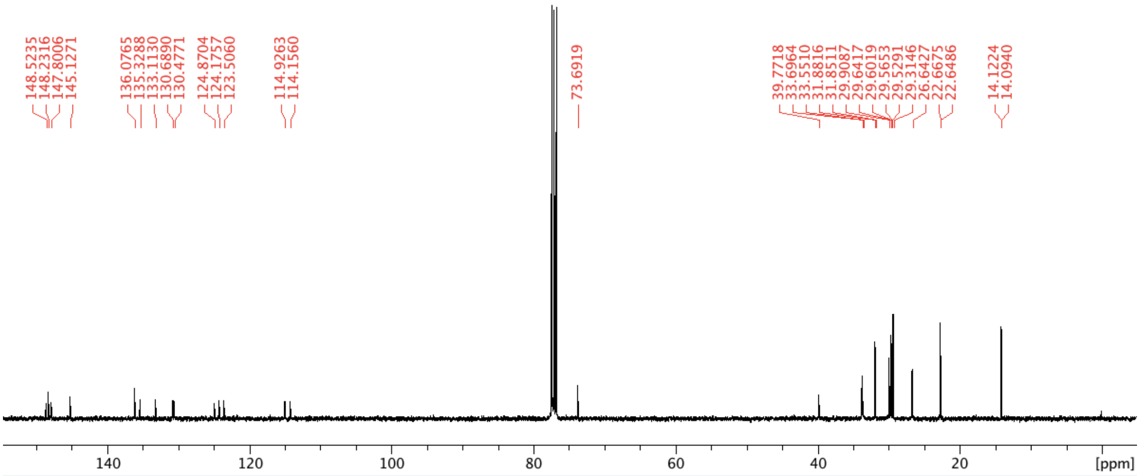
148.5235
148.2316
147.8006
145.1271
136.0765
135.3288
133.1130
130.6890
130.4771
124.8704
124.1757
123.5060
114.9263
114.1560
73.6919
39.7718
33.6964
33.5510
31.8816
31.8511
29.9087
29.6417
29.6019
29.5653
29.5291
29.3146
26.6427
22.6675
22.6486
14.1224
14.0940
140
120
100
80
60
40
20
[ppm]

Diiodo-Core (2)

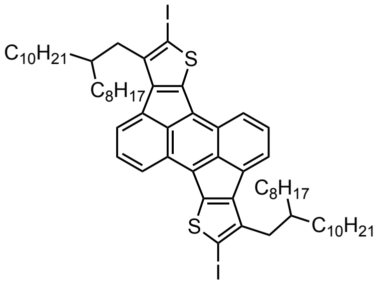

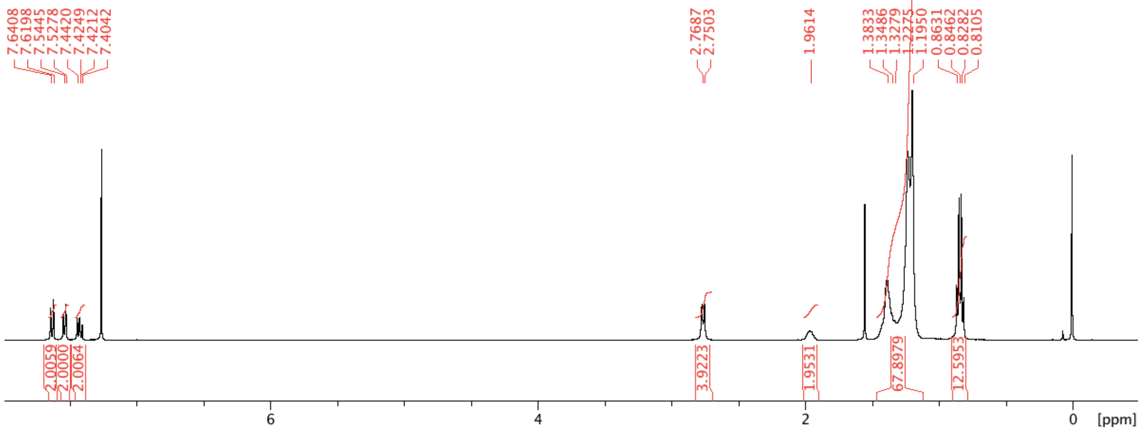

BisTCNE

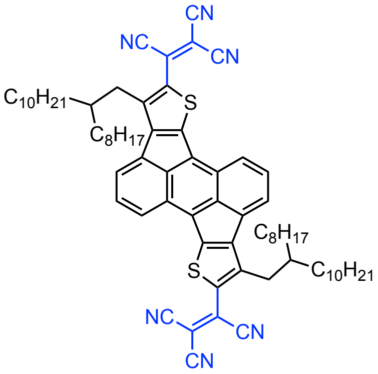
CN
NC
CN
$C_{10}H_{21}$
S
C_8H_{17}
C_8H_{17}
$C_{10}H_{21}$
S
NC
CN
CN

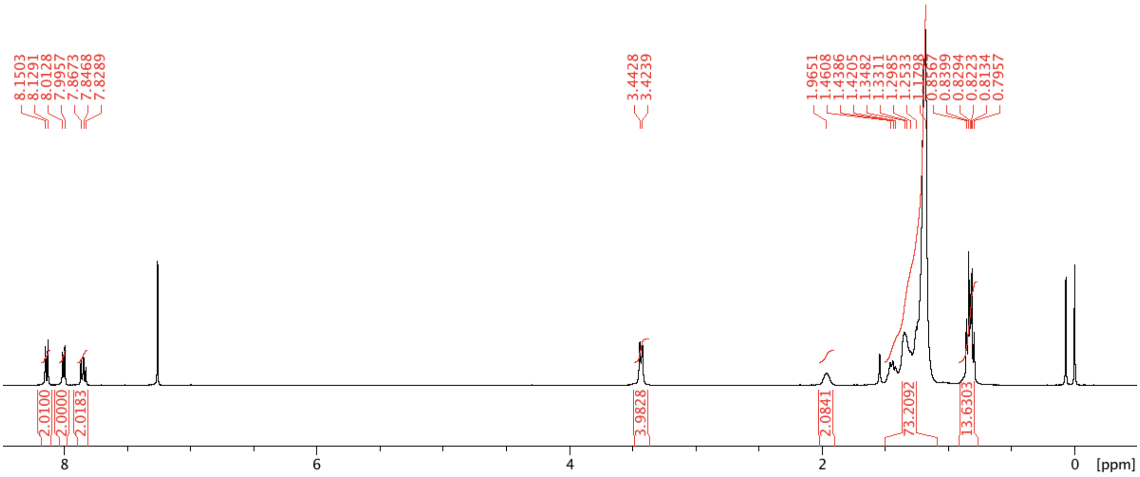
8.1503
8.1291
8.0128
7.9957
7.8673
7.8468
7.8289
3.4428
3.4239
1.9651
1.4608
1.4386
1.4205
1.3482
1.3311
1.2985
1.2533
1.1798
0.8567
0.8399
0.8294
0.8223
0.8134
0.7957
2.0100
2.0000
2.0183
3.9828
2.0841
73.2092
13.6303
8
6
4
2
0
[ppm]

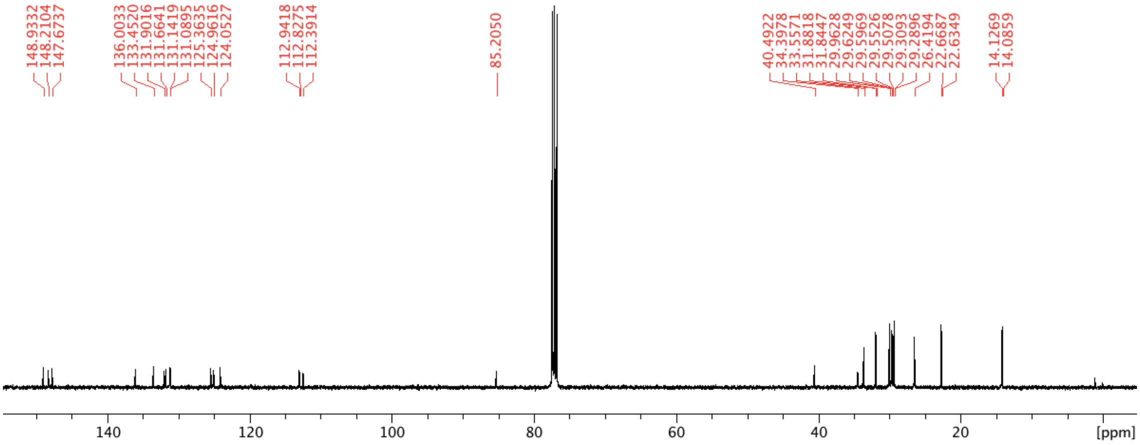
148.9332
148.2104
147.6737
136.0033
133.4520
131.9016
131.6641
131.1419
131.0895
125.3635
124.9616
124.0527
112.9418
112.8275
112.3914
85.2050
40.4922
34.3978
33.5571
31.8818
31.8447
29.9628
29.6249
29.5969
29.5526
29.5078
29.3093
29.2896
26.4194
22.6687
22.6349
14.1269
14.0859
140
120
100
80
60
40
20
[ppm]

Dibromo-Core (3)

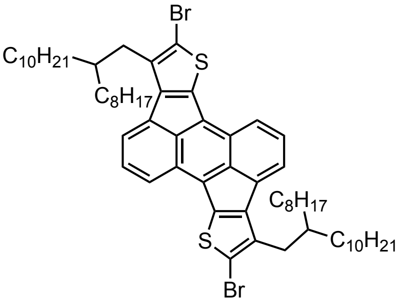

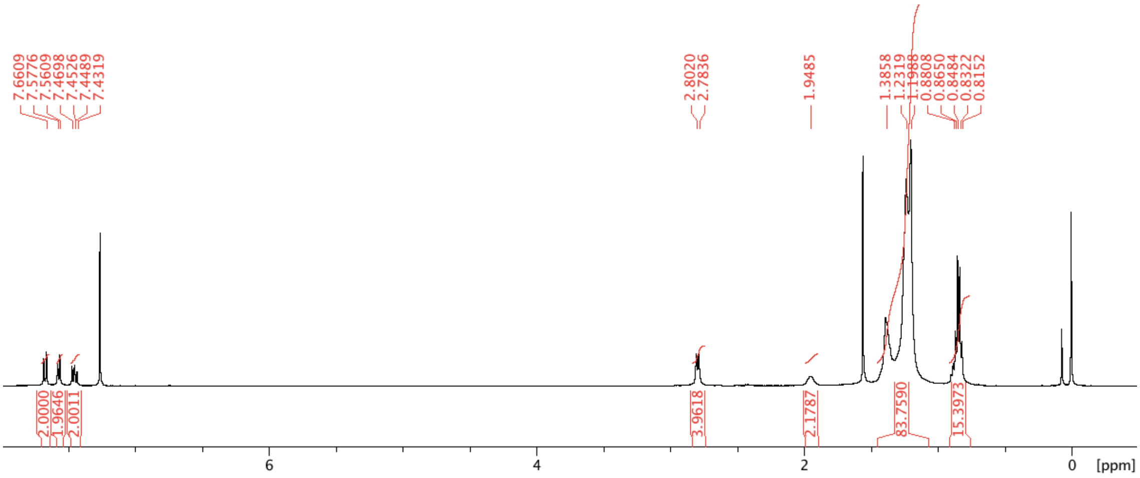

TCNQE

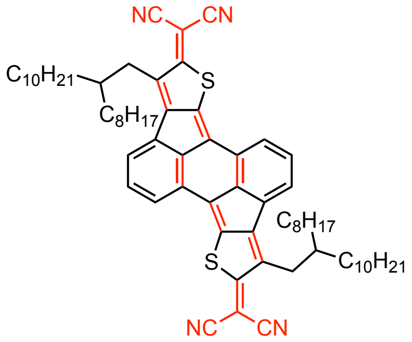
NC
CN
S
C10H21
C8H17
C8H17
C10H21
S
NC
CN

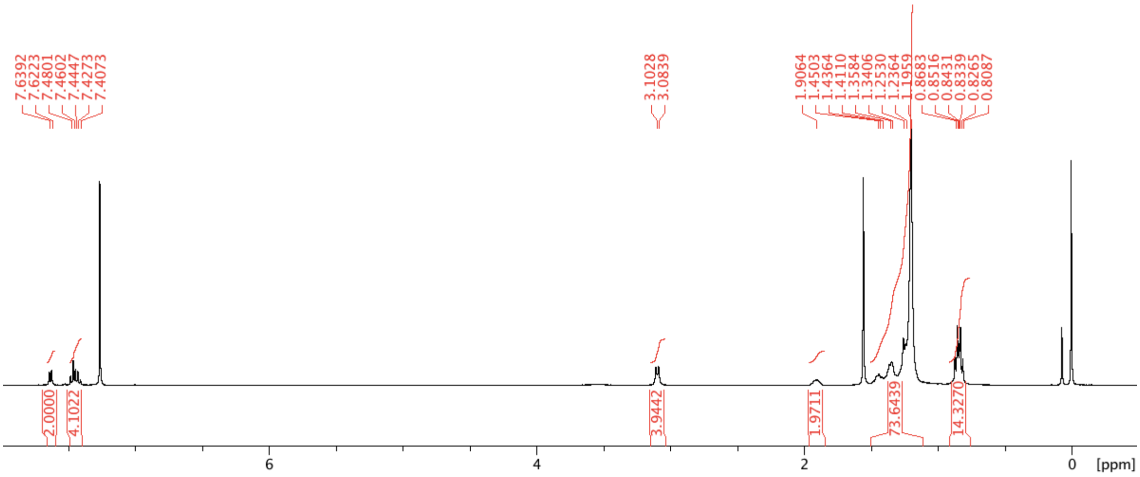
7.6392
7.6223
7.4801
7.4602
7.4447
7.4273
7.4073
3.1028
3.0839
1.9064
1.4503
1.4364
1.4110
1.3584
1.3406
1.2530
1.2364
1.1959
0.8683
0.8516
0.8431
0.8339
0.8265
0.8087
2.0000
4.1022
3.9442
1.9711
73.6439
14.3270
6
4
2
0
[ppm]

S8. Reference

1 Gaussian 09W, Revision C.01, M. J. Frisch, G. W. Trucks, H. B. Schlegel, G. E. Scuseria, M. A. Robb, J. R. Cheeseman, G. Scalmani, V. Barone, B. Mennucci, G. A. Petersson, H. Nakatsuji, M. Caricato, X. Li, H. P. Hratchian, A. F. Izmaylov, J. Bloino, G. Zheng, J. L. Sonnenberg, M. Hada, M. Ehara, K. Toyota, R. Fukuda, J. Hasegawa, M. Ishida, T. Nakajima, Y. Honda, O. Kitao, H. Nakai, T. Vreven, J. A. Montgomery, Jr., J. E. Peralta, F. Ogliaro, M. Bearpark, J. J. Heyd, E. Brothers, K. N. Kudin, V. N. Staroverov, T. Keith, R. Kobayashi, J. Normand, K. Raghavachari, A. Rendell, J. C. Burant, S. S. Iyengar, J. Tomasi, M. Cossi, N. Rega, J. M. Millam, M. Klene, J. E. Knox, J. B. Cross, V. Bakken, C. Adamo, J. Jaramillo, R. Gomperts, R. E. Stratmann, O. Yazyev, A. J. Austin, R. Cammi, C. Pomelli, J. W. Ochterski, R. L. Martin, K. Morokuma, V. G. Zakrzewski, G. A. Voth, P. Salvador, J. J. Dannenberg, S. Dapprich, A. D. Daniels, O. Farkas, J. B. Foresman, J. V. Ortiz, J. Cioslowski, and D. J. Fox, Gaussian, Inc., Wallingford CT, 2010.